

## Direct observation of magnetic proximity effects in amorphous exchange-spring magnets by neutron reflectometry

A. J. Qviller <sup>\*</sup>, C. Frommen, and B. C. Hauback

*Institute for Energy Technology, P.O. Box 40, NO-2027 Kjeller, Norway*

F. Magnus

*Division for Materials Physics, Department of Physics and Astronomy, Uppsala University, Box 516, SE-751 20 Uppsala, Sweden  
and Science Institute, University of Iceland, Dunhaga 3, 107 Reykjavik, Iceland*

B. J. Kirby

*Center for Neutron Research, NIST, Gaithersburg, Maryland 20899, USA*

B. Hjörvarsson

*Division for Materials Physics, Department of Physics and Astronomy, Uppsala University, Box 516, SE-751 20 Uppsala, Sweden*



(Received 10 April 2018; revised 27 May 2020; accepted 22 September 2020; published 7 October 2020)

In this paper, we report a direct observation of a magnetic proximity effect in an amorphous thin-film exchange-spring magnet by the use of neutron reflectometry. The exchange-spring magnet is a trilayer consisting of two ferromagnetic layers with high  $T_c$  separated by a ferromagnetic layer, which is engineered to have a significantly lower  $T_c$  than the embedding layers. This enables us to measure magnetization depth profiles at which the low- $T_c$  material is in a ferromagnetic or paramagnetic state, while the embedding layers are ferromagnetic. A clear proximity effect is observed 7 K above the intrinsic  $T_c$  of the embedded layer, with a range extending 50 Å.

DOI: [10.1103/PhysRevMaterials.4.104404](https://doi.org/10.1103/PhysRevMaterials.4.104404)

Magnetic proximity effects can be prominent at interfaces [1]. These interface effects are present in a variety of magnetic thin films and heterostructures, often having profound effects on the observed magnetic properties [2,3]. As an example, proximity effects in nonmagnetic spacer layers separating two ferromagnets can give rise to long-range interlayer exchange coupling [4], changes in ordering temperature [5], and/or nonoscillatory alignment of magnetic layers [6,7]. Since layered magnetic structures are ubiquitous in modern technology, the understanding of magnetic proximity effects is of fundamental importance.

In this paper, we investigate the proximity effect in a ferromagnet-paramagnet system, more specifically in a trilayer [8] of an amorphous exchange-spring magnet [3]. Amorphous heterostructures are free of atomic step edges and grain boundaries and can therefore have well-defined and smooth layers [9]. The exchange-spring magnet investigated here consists of three ferromagnetic layers, shown schematically in Fig. 1. The top  $\text{Co}_{85}(\text{AlZr})_{15}$  layer (A) has an intrinsic  $T_c$  well above room temperature and a small imprinted uniaxial anisotropy obtained as described in Refs. [3,10]. The middle layer (B), which is magnetically isotropic  $\text{Co}_{60}(\text{AlZr})_{40}$ , is engineered to have a  $T_c$  well below room temperature, much lower than the other layers. The bottom layer (C) consists of  $\text{Sm}_8\text{Co}_{92}$ , which has a  $T_c$  well above room temperature. Layer C has a large imprinted

anisotropy, which can, e.g., be used to increase the magnetic coercivity of the adjacent layers. This type of sample structure has previously been used to indirectly demonstrate that a proximity-induced magnetization exists in layer B well above its intrinsic ordering temperature  $T_c^B$  [3]. The inferred proximity effect was observed to result in an exchange-spring behavior at temperatures 50% above  $T_c^B$  and an exchange bias at even higher temperatures. However, no direct information concerning the magnetic state of the center layer was provided. Here we present direct evidence of an induced magnetization in the low- $T_c$  middle layer and we also infer the magnetic profile throughout the layers, using polarized neutron reflectivity measurements [11]. In particular, polarized neutron reflectivity measurements return the absolute magnetic moment and thus complement the results obtained by x-ray resonant magnetic scattering described in Ref. [3].

The samples were grown by dc magnetron sputtering in a UHV sputtering chamber at an Ar (99.9999% purity) sputtering gas pressure of 0.27 kPa. First, a 20-Å-thick seeding layer of  $\text{Al}_{70}\text{Zr}_{30}$  was deposited on a Si(100) substrate (with the native oxide) from an  $\text{Al}_{70}\text{Zr}_{30}$  alloy target of purity 99.9%. Subsequently, a 200-Å-thick  $\text{Sm}_8\text{Co}_{92}$  alloy film was grown by cosputtering from elemental targets of Co (99.9% purity) and Sm (99.9% purity), after which a  $\text{Co}_{60}(\text{Al}_{70}\text{Zr}_{30})_{40}$  of 100 Å and a  $\text{Co}_{85}(\text{Al}_{70}\text{Zr}_{30})_{15}$  layer of 150 Å were grown by cosputtering from the Co and AlZr targets. Finally, a 30-Å-thick capping layer of  $\text{Al}_{70}\text{Zr}_{30}$  was grown to protect the underlying magnetic trilayer from oxidation. All films were grown at room temperature and were

<sup>\*</sup>Corresponding author: [atlej@atlejq@gmail.com](mailto:atlej@atlejq@gmail.com)

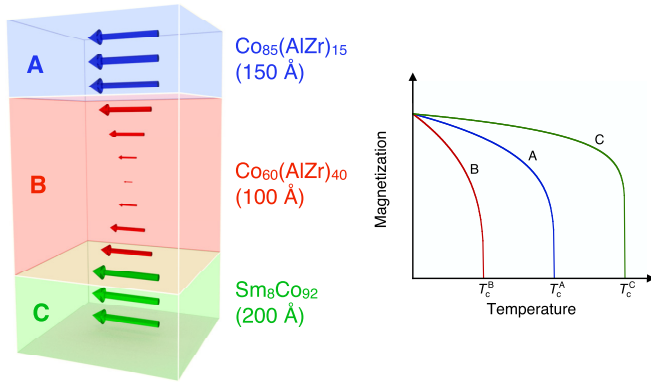


FIG. 1. A schematic representation of the amorphous trilayer and an inferred magnetic proximity effect. The arrows denote the size of the magnetic moments. Layers A and C have a high magnetic ordering temperature whereas layer B has a low ordering temperature as shown on the right. As illustrated in the figure, a pronounced proximity-induced magnetization in layer B is expected at temperatures above  $T_c^B$ . Figure adapted from Ref. [3].

not heated above room temperature to avoid interdiffusion of the layers. Two permanent magnets provided a magnetic field of approximately 0.1 T parallel to the plane of the films during growth as described in Ref. [10]. This induces a uniaxial in-plane anisotropy in the ferromagnetic layers having an ordering temperature above the growth temperature (A and C). The atomic flux as a function of magnetron power was determined for each target material through x-ray reflectivity measurements of films grown using each of the magnetrons. The power on each magnetron was then set to achieve a given composition while cosputtering. Rutherford backscattering spectrometry previously confirmed that this is a robust method for the materials in question [12,13]. Magneto-optical Kerr effect (MOKE) measurements were carried out on the samples to confirm the  $T_c$  of the middle layer and that the magnetization loops of the trilayers were consistent with previously studied samples. More details on the growth and structural characterization can be found in Refs. [3,10,14,15]. Notably, the use of x-ray reflectivity measurements in Ref. [14] shows that the growth methodology results in well-defined boundaries of the layers, returning a 4 Å root mean square (RMS) interface roughness and thus ruling out significant interdiffusion even for interlayers as thin as 25 Å. Susceptibility measurements did not provide any useful signal from a change in magnetization of the center layer.

Polarized neutron reflectivity experiments were carried out at the PBR beamline at NIST at a wavelength of  $\lambda = 4.75$  Å using an instrument resolution of  $\Delta\lambda/\lambda = 0.01$ . Four reflectivities, corresponding to the two non-spin-flip channels ( $R^{++}$  and  $R^{--}$ ) as well as the two spin-flip channels ( $R^{-+}$  and  $R^{+-}$ ), were measured out to  $q = 0.2$  Å<sup>-1</sup> at  $T_1 = 300$  K,  $T_2 = 110$  K, and  $T_3 = 10$  K. With  $T_c^B = 103 \pm 1$  K [3] (see Fig. 1), these temperatures correspond to  $T_1 \gg T_c^B$ ,  $T_2 > T_c^B$ , and  $T_3 < T_c^B$ . Samples were measured with an applied external field of  $\mu_0 H = 10$  mT along the easy axis of the imprinted anisotropy and the scattering plane perpendicular to this axis. Measurements of the spin-flip reflectivities returned mainly noise, consistent with the presence of a collinear magnetic

state [11], which is reasonable in the given measurement configuration. The spin-flip reflectivities were therefore subsequently disregarded in the fitting process.

Data were fitted using the GENX 2.4.7 reflectivity package with the new MagRefl module [16], using the logarithm of the reflectivity as the figure of merit. The sample model consists of a partially oxidized capping layer (oxide consisting of a 70/30 mixture of Al<sub>2</sub>O<sub>3</sub>/ZrO<sub>2</sub> and a Al<sub>70</sub>Zr<sub>30</sub> layer), a magnetic Co<sub>85</sub>(AlZr)<sub>15</sub> layer, a magnetic Co<sub>60</sub>(AlZr)<sub>40</sub> interlayer, a magnetic Sm<sub>8</sub>Co<sub>92</sub> layer, and a seeding layer of Al<sub>70</sub>Zr<sub>30</sub> on a thin SiO<sub>2</sub> layer on a Si substrate (see Fig. 3). Most structural parameters were determined by fitting the results obtained at  $T = 300$  K and  $\mu_0 H = 10$  mT. Reflectivity measurements are not sufficient to uniquely determine the chemical composition of layers consisting of more than two elements, but the validation of the sample preparation procedure stated above justifies fixing the stoichiometry of the layers to the intended values and only allowing their densities to vary during the fitting at  $T = 300$  K and  $\mu_0 H = 10$  mT. In the simulations, the low- $T_c$  layer was defined by ten slices and the total magnetic moment of these layers were fitted to a sum of two power laws with the same exponent, corresponding to a decaying magnetization from each interface, induced by the neighboring ferromagnetic layers as illustrated in Fig. 1. A power-law decay of the magnetization was chosen as it is the functional form of the long-range exchange interaction, as, e.g., described in Refs. [3,17]. The resulting stepwise magnetic profile was smoothed by allowing a small, linked chemical interface width (7 Å RMS) for each slice. Only the magnetization of the three ferromagnetic layers and their profiles were allowed to vary when fitting the data obtained at  $T = 110$  K and  $T = 10$  K. Changes in layer thickness were needed to account for the thermal expansion in the layers, which was determined to be  $4.1 \times 10^{-5}$  K<sup>-1</sup>, or 1.2% when heating the sample from  $T = 10$  K to  $T = 300$  K. Notice that the determined thermal expansion only holds for the combined film and substrate, where the substrate provides an elastic boundary defining the changes in the lateral direction with temperature, due to clamping effects. The resulting polarized neutron reflectivity results (scaled in  $q$ ) and corresponding fits are shown in Figs. 2(a)–2(c).

The determined chemical and magnetic scattering length density (SLD) profiles at  $T = 300$  K and  $\mu_0 H = 10$  mT are shown in Fig. 3(a), as functions of the distance from the substrate ( $z$ ). Both the  $R^{++}$  and the  $R^{--}$  fits at  $T = 300$  K are of good quality and yield a chemical SLD profile with interface widths equal to or less than 8 Å RMS. In particular, for layers A, B and C widths were found to be in the range 6 – 8 Å RMS. The results from the fits of polarized neutron reflectivity data described in Ref. [14] agree almost perfectly with the ones presented here. Furthermore, the analysis of neutron reflectivity were found to return slightly larger interface widths (6 Å RMS) than the x-ray reflectivity results (4 Å RMS) [14].

The inferred magnetic SLD profiles are shown in Fig. 3(b). At  $T = 300$  K and  $\mu_0 H = 10$  mT (green line), no magnetization is observed in layer B. Furthermore, the magnetization at the interfaces decays sharply, consistent with relatively short-ranged magnetic interface effects at that temperature. At the lowest temperature,  $T = 10$  K (black line), the middle

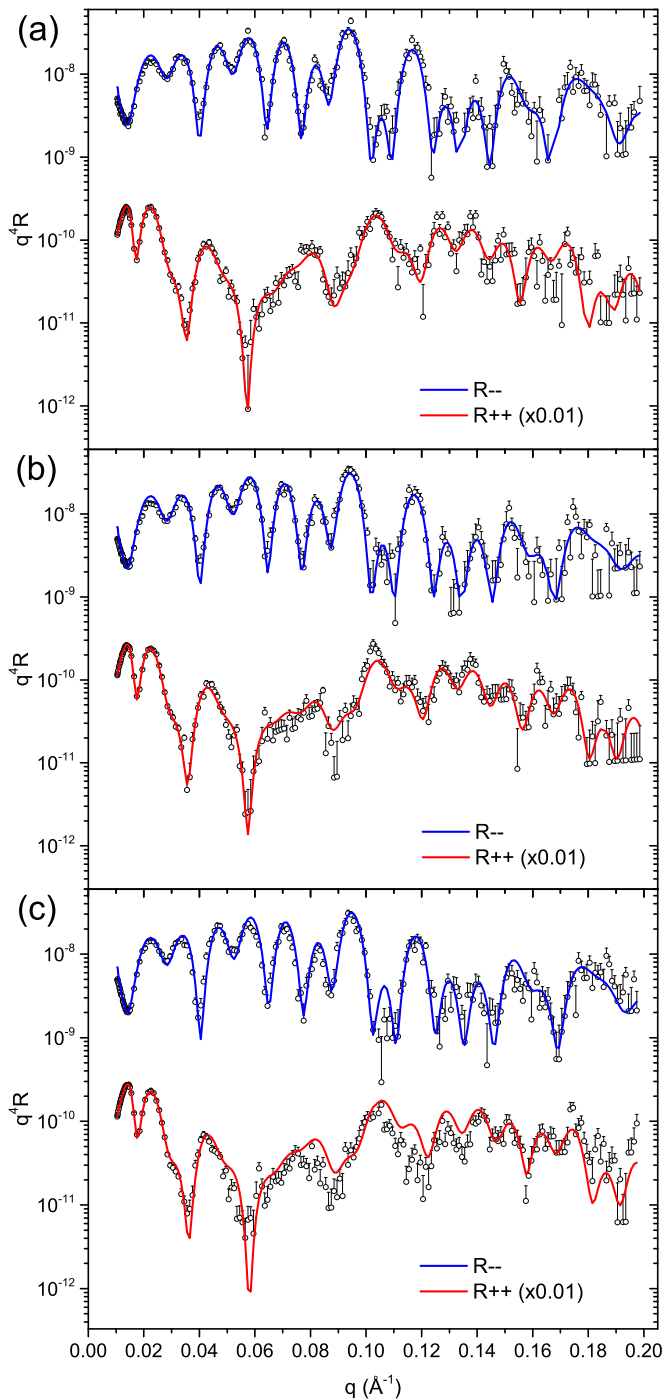


FIG. 2. Non-spin-flip-polarized neutron reflectivity scans,  $R^{--}$  and  $R^{++}$ , measured at  $\mu_0 H = 10$  mT and (a)  $T = 300$  K, (b)  $T = 110$  K, and (c)  $T = 10$  K. Fits are shown as solid lines in red and blue. Error bars correspond to  $\pm 1$  standard deviation and are shown only on the upper side for clarity.

layer is magnetized, as expected, since this is well below the ordering temperature of that layer. Significant magnetic SLD is seen throughout layer B at  $T = 110$  K (red line) which is well above the ordering temperature (7 K above  $T_c^B$ ). The uncertainty in the magnetic SLD of layer B was estimated by inspection of how much it can be altered before the fits become visually worse. This limit was found to be

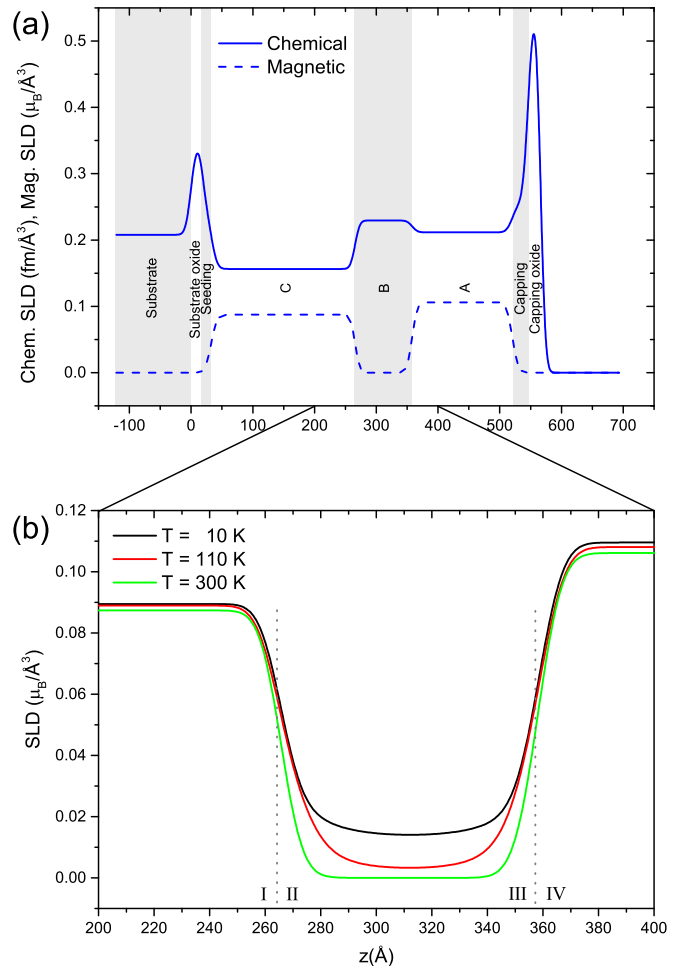


FIG. 3. (a) Chemical and magnetic SLD profiles at  $\mu_0 H = 10$  mT and  $T = 300$  K for the entire exchange-spring magnet heterostructure. The capping layer, layers A, B, C, the seeding layer, and the substrate are indicated. Oxide layers on the capping layer and substrate are also marked. (b) Magnetization profiles of the low- $T_c$   $\text{Co}_{60}(\text{AlZr})_{40}$  middle layer and its interfaces at  $\mu_0 H = 10$  mT,  $T = 10, 110,$  and  $300$  K. Error bars (not shown) of the magnetization in the center of this layer are 7% for all temperatures. The magnetization profiles at  $T = 10$  K and  $110$  K have been offset to correct for the measured thermal expansion.

7% for both the  $T = 10$  K data and the  $T = 110$  K data. For technical reasons, the latter uncertainty was also used for the magnetic SLD at  $T = 300$  K. The  $R^{++}$  fit at  $T = 10$  K has some uncertainty, but the fitting process always returns zero magnetic SLD in the center of layer B at  $T = 300$  K, weak magnetization in layer B at  $T = 110$  K, and significant magnetization in layer B at  $T = 10$  K for a large number of attempted models. It is therefore believed that the results are robust and conclusive. Thus, having as much as  $\approx 1/4$  of the magnetic SLD retained well above the intrinsic ordering temperature of the layer can be viewed as a strong manifestation of a long-range magnetic proximity effect. However, we need to have a closer look on the changes in the magnetic profile to obtain a better understanding of the roots of the inferred proximity effects.

TABLE I. Absolute value of the half-width half maxima of the derivative of the magnetic SLD profiles.

| Temperature (K) | I (Å) | II (Å) | III (Å) | IV (Å) |
|-----------------|-------|--------|---------|--------|
| $10 \pm 1$      | 7.3   | 8.7    | 9.1     | 8.3    |
| $110 \pm 1$     | 8.3   | 12     | 12      | 8.6    |
| $300 \pm 1$     | 7.4   | 7.3    | 9.1     | 7.9    |

As there is a significant magnetization in the center of the 100-Å-thick layer B well above  $T_c^B$ , the range of the proximity effects can be inferred to be at least 50 Å at  $T = 110$  K, consistent with the presence of long-range effective exchange interactions [3]. Beside these long-range effects, the width of the magnetic interface is changing as seen in the changes of the SLD, displayed in Fig. 3(b). Four half-widths at half maxima were determined, describing the spatial change in magnetization at the interfaces of the layers. The choice of half widths at half maxima as a measure arises from the need to capture the expected asymmetry in the magnetic profiles. The results are provided in Table I, the annotations of the interfaces I–IV are defined in Fig. 3(b). The widths I and IV describe the change in the magnetization of the outer boundaries of layers A and C. These are found to be independent of temperature.

The changes in width II (III) describe the changes in the magnetization profile of the interface of A (C) and B. At  $T = 10$  K, all the layers are close to being fully magnetic and the deduced magnetic SLD therefore resembles primarily the distribution of the elements in the sample. The width of the interface includes intermixing and roughness of the layers, which are indistinguishable in specular reflectivity and independent of temperature. At  $T = 300$  K, the magnetization and susceptibility of layer B are negligible and the width is therefore dominated by the elemental distribution and interface effects in layers A and C. Thus the widths of the magnetic profile obtained at these temperatures are expected to be similar, as the ordering temperature is much higher than room temperature. We also note the center of the distribution is unchanged with temperature. The width of the magnetic profile in regions II and III is clearly larger at  $T = 110$  K as compared to the other temperatures, as seen in Fig. 3(b) and Table I. To underpin the above analysis, a normal probability plot of the values in Table I was done (not shown). It revealed that the widths of regions II and III at  $T = 110$  K are outliers at  $2.0 \sigma$ , while the rest of the observations are approximately normally distributed around a sample mean of 8.8 Å, again

consistent with the previous discussion of chemical interface widths. The decay of the magnetic SLD at  $T = 110$  K is therefore consistent with the presence of short-ranged magnetic proximity effects at the interfaces between A (C) and B.

The above discussion is based upon interface effects arising from the temperature-dependent magnetic susceptibility at and above  $T_c$ . Monte Carlo simulations involving beyond-nearest-neighbor interactions show that not only is the calculated peak in the magnetic susceptibility shifted to higher temperature, it is also significantly broadened due to proximity effects [3]. Furthermore, an extended region of induced magnetization can be expected in layer B, when interactions are beyond nearest neighbor. However, independent of the range of interactions, there will be a decay in the magnetization with increasing distance from the interface. It is therefore difficult to rationalize the observed constant level in the magnetic SLD in layer B at  $T = 110$  K using these ideas.

The influence of the elemental distribution in random alloys on magnetic properties was recently addressed using atomic probe measurements [18]. The change in the effective exchange coupling with concentration ( $\delta T_c / \delta c \propto \delta J / \delta c$ ) [18] was used to develop a description of the magnetic properties of random alloys. For example, the results were used to describe unusual thickness dependence of the ordering temperature in the extreme thin limit [19,20] and the resulting magnetic susceptibility above  $T_c$  in the thin layer limit [21]. The most important consequence of the inhomogeneous spatial distribution of the elements (random) is the formation of dynamic wormlike magnetic features. The size of these features is limited by the effective cutoff in magnetic coupling, defined by changes in the *local* chemical composition and the temperature [18]. When in contact with layers A and C, these can be polarized, retaining a net magnetization, from a pinning at the interfaces. We therefore argue that the obtained proximity effects have two origins: (1) short-ranged magnetic interface effects and (2) magnetization arising from random and dynamic magnetic networks, pinned by the magnetic interactions at the interfaces. These findings open up questions concerning interface effects, which could have large a impact on our understanding and design of layered magnetic materials.

The Research Council of Norway is acknowledged for financial support through the SYNKNØYT program, Project No. 218418. This work was also funded by the Swedish Research Council (VR) and the Knut and Alice Wallenberg Foundation (KAW). F.M. acknowledges funding from the Icelandic Research Fund Grant No. 174271-051. A.J.Q. would like to express his gratitude to Bengt Lindgren for his skilful assistance with modeling in GenX.

- [1] R. M. White and D. J. Friedman, Theory of the magnetic proximity effect, *J. Magn. Magn. Mater.* **49**, 117 (1985).
- [2] P. K. Manna and S. M. Yusuf, Two interface effects: Exchange bias and magnetic proximity, *Phys. Rep.* **535**, 61 (2014).
- [3] F. Magnus, M. E. Brooks-Bartlett, R. Moubah, R. A. Procter, G. Andersson, T. Hase, S. T. Banks, and B. Hjörvarsson, Long-range magnetic interactions and proximity effects in an

amorphous exchange-spring magnet, *Nat. Commun.* **7**, 11931 (2016).

- [4] N. J. Gökemeijer, T. Ambrose, and C. L. Chien, Long-Range Exchange Bias Across a Spacer Layer, *Phys. Rev. Lett.* **79**, 4270 (1997).
- [5] U. Bovensiepen, F. Wilhelm, P. Srivastava, P. Pouloupoulos, M. Farle, A. Ney, and K. Baberschke, Two Susceptibility Maxima

- and Element Specific Magnetizations in Indirectly Coupled Ferromagnetic Layers, *Phys. Rev. Lett.* **81**, 2368 (1998).
- [6] W. L. Lim, N. Ebrahim-Zadeh, J. C. Owens, H. G. E. Hentschel, and S. Urazhdin, Temperature-dependent proximity magnetism in Pt, *Appl. Phys. Lett.* **102**, 162404 (2013).
- [7] M. Gottwald, J. J. Kan, K. Lee, S. H. Kang, and E. E. Fullerton, Paramagnetic  $\text{Fe}_x\text{Ta}_{1-x}$  alloys for engineering of perpendicularly magnetized tunnel junctions, *APL Mater.* **1**, 022102 (2013).
- [8] E. E. Fullerton, J. S. Jiang, M. Grimsditch, C. H. Sowers, and S. D. Bader, Exchange-spring behavior in epitaxial hard/soft magnetic bilayers, *Phys. Rev. B* **58**, 12193 (1998).
- [9] C.-M. Choi, J.-O. Song, and S.-R. Lee, Thermal stability of magnetic tunnel junctions with new amorphous ZrAl-alloy films as the under and capping layers, *IEEE T. Magn.* **41**, 2667 (2005).
- [10] H. Raanaei, H. Nguyen, G. Andersson, H. Lidbaum, P. Korelis, K. Leifer, and B. Hjörvarsson, Imprinting layer specific magnetic anisotropies in amorphous multilayers, *J. Appl. Phys.* **106**, 023918 (2007).
- [11] H. Zabel, X-ray and neutron reflectivity analysis of thin films and superlattices, *Appl. Phys. A* **58**, 159 (1994).
- [12] A. Liebig, P. T. Korelis, H. Lidbaum, G. Andersson, K. Leifer, and B. Hjörvarsson, Morphology of amorphous  $\text{Fe}_{91}\text{Zr}_9/\text{Al}_2\text{O}_3$  multilayers: Dewetting and crystallization, *Phys. Rev. B* **75**, 214202 (2007).
- [13] A. Frisk, F. Magnus, S. George, U. B. Arnalds, and G. Andersson, Tailoring anisotropy and domain structure in amorphous TbCo thin films through combinatorial methods, *J. Phys. D: Appl. Phys.* **49**, 035005 (2016).
- [14] K. A. Thórarinsdóttir, H. Palonen, G. K. Palsson, B. Hjörvarsson, and F. Magnus, Giant magnetic proximity effect in amorphous layered magnets, *Phys. Rev. Materials* **3**, 054409 (2019).
- [15] F. Magnus, R. Moubah, A. H. Roos, A. Kruk, V. Kapaklis, T. Hase, B. Hjörvarsson, and G. Andersson, Tunable giant magnetic anisotropy in amorphous SmCo thin films, *Appl. Phys. Lett.* **102**, 162402 (2013).
- [16] M. Björck and G. Andersson, GenX: An extensible x-ray reflectivity refinement program utilizing differential evolution, *J. Appl. Crystallogr.* **40**, 1174 (2007).
- [17] M. E. Fisher, S. Ma, and B. G. Nickel, Critical Exponents for Long-Range Interactions, *Phys. Rev. Lett.* **29**, 917 (1972).
- [18] R. Gemma, M. to Baben, A. Pundt, V. Kapaklis, and B. Hjörvarsson, The impact of nanoscale compositional variation on the properties of amorphous alloys, *Sci. Rep.* **10**, 11410 (2020).
- [19] P. T. Korelis, P. E. Jönsson, A. Liebig, H.-E. Wannberg, P. Nordblad, and B. Hjörvarsson, Finite-size effects in amorphous  $\text{Fe}_{90}\text{Zr}_{10}/\text{Al}_{75}\text{Zr}_{25}$  multilayers, *Phys. Rev. B* **85**, 214430 (2012).
- [20] A. Liebig, P. T. Korelis, M. Ahlberg, and B. Hjörvarsson, Experimental realization of amorphous two-dimensional XY magnets, *Phys. Rev. B* **84**, 024430 (2011).
- [21] M. Ahlberg, G. Andersson, and B. Hjörvarsson, Two-dimensional XY-like amorphous  $\text{Co}_{68}\text{Fe}_{24}\text{Zr}_8/\text{Al}_{70}\text{Zr}_{30}$  multilayers, *Phys. Rev. B* **83**, 224404 (2011).